COUPLED IN-ROCK AND IN-DRIFT HYDROTHERMAL MODEL STUDY FOR YUCCA MOUNTAIN

G. Danko[1], J. Birkholzer[2], D. Bahrami[1]

Total number of pages (including this page):   1

Total number of figures: 11

Total number of tables: 13

[1]Department of Mining Engineering, University of Nevada Reno

[2]Lawrence Berkeley National Laboratory (LBNL)

Person to whom proofs and page charge are to be sent:

Dr. George Danko

Mailing Address:

University of Nevada, Reno

1664 North Virginia Street, Mail stop 173

Reno, NV 89557

Phone: (775)784-4284

Fax: (775)784-4284

Email: danko@unr.edu

ABSTRACT

A thermal-hydrologic-natural-ventilation model is configured for simulating temperature, humidity, and condensate distributions in the coupled domains of the in-drift airspace and the near-field rockmass in the proposed Yucca Mountain repository. The multi-physics problem is solved with MULTIFLUX in which a lumped-parameter computational fluid dynamics model is iterated with TOUGH2. The solution includes natural convection, conduction, and radiation for heat as well as moisture convection and diffusion for moisture transport with half waste package scale details in the drift, and mountain-scale heat and moisture transport in the porous and fractured rock-mass. The method provides fast convergence on a personal computer computational platform. Numerical examples and comparison with a TOUGH2 based, integrated model are presented.

KEYWORDS

Nuclear waste, permanent storage, MULTIFLUX model

INTRODUCTION

Numerical model and solution method improvement are underway with the purpose of improving understanding of the coupling between thermo-hydrological processes (including air and vapor movement) in the in-drift, near-field, and mountain-scale systems at the proposed Yucca Mountain (YM) repository. Specific aims are (1) to configure, test, and verify a novel, efficient, numerical-computational, coupled model; and (2) to evaluate the coupled, in-drift heat and moisture transport with evaporation, condensation, and seepage of water into drifts from the near-field rockmass at different stages after waste emplacement. These objectives are met by appling a multi-scale modeling approach that (1) integrates in-drift and in-rock process models in a consistent, transparent, and scientifically defensible manner; and (2) allows for studying the storage environment in various emplacement drifts without applying excessive conservatism in the modeling assumptions.

Model improvement, testing, and application follow several years of development of MULTIFLUX (MF), which started with the application of a coupled thermal-hydrologic and ventilation model for YM[1]. The heat, moisture and air transport processes in the near-field rock mass and in the emplacement drift space are modeled with two distinct and specific model elements. The two sub-models are re-coupled during the conjugate numerical solution in MF. The distinct model-elements are (1) the multi-phase porous-medium simulator TOUGH2[2] for the in-rock processes around the drift in the unsaturated zone; and (2) a lumped-parameter Computational Fluid Dynamic (CFD) model for the in-drift transport processes, including natural air convection and condensation around the waste packages. Re-coupling of these distinct model-elements is made by a novel, iterative coupler that enforces boundary coupling of the heat and moisture transport processes on the interface between the drift air space and the rockmass. MF applies an innovative, surrogate model-element, obtained from a Numerical Transport Code

Functionalization (NTCF) procedure[3], for reducing the number of TOUGH2 runs during iteration.

The need for applying a CFD model-element for the in-drift processes lies in the facts that (1) turbulent flow and transport are expected in the emplacement drifts for thousands of years; (2) non-linear, convective air currents dominantly affect the flow of heat and moisture; (3) the thermal connections are highly unstructured due to three-dimensional heat radiation in an engineered system; and (4) that the model discretization must follow a strongly heterogeneous design geometry. Conventional CFD models, however, require large computational capacity and time for the simulation of a single drift at one time instant, e.g, one million nodes and two weeks run time on a supercomputer. They also require iteration on the air-rock interface with the rockmass model since neither Dirichlet nor Newman (flux) boundary condition can be prescribed *a priori* for the solution. Such iteration however, has not been implemented in any of the conventional CFD model applications for YM.[4,5,6] Considering the excessive computational time for both the conventional CFD solution and the porous-media rockmass solution, the prospect of reaching a coupled, conjugate solution by iteration is a challenging task that has yet to be solved. The published CFD model results to date are, therefore, useful mainly for the purpose of evaluation of turbulent mixing and transport properties for the air space model domain. [4,5]

Solutions have been published to approximate the transport processes in the in-drift model domain with an equivalent porous-medium model-element. By doing this, the in-rock and in-drift domains can be solved together in a direct procedure by using fast-converging, proven numerical techniques. Buscheck et al.[7] applied an iterative adjustment process in NUFT for the evaluation of thermal conductivity and permeability in the porous-medium model against an outside CFD calculation[8]. Birkholzer et al.[9,15] investigated axial transport of moisture and heat

along a representative emplacement drift using a porous-media implementation of the in-drift processes in TOUGH2. These simplified solution approaches, however, leave the questions open as to how good the porous-medium approximation compares to a more detailed representation of the time-dependent in-drift mixing processes.

The lumped-parameter CFD model choice for the in-drift domain in MF provides strategic advantages. Firstly, it incorporates the mass, energy and momentum balances in the emplacement drift in several thousand locations, but does not solve for all the flow details. The approach used in MF allows for saving computational time and resources by applying known solutions from literature or importing input data only sparingly from an outside, parallel CFD solution. The time-honored transport coefficients may be readily used in the model configuration. Secondly, the reduced computational workload with the lumped-parameter CFD approach allows for the re-calculation of critical heat and mass fluxes in the emplacement drift during iteration with the rockmass model-element. In the present application, support data for in-drift airflow distribution, and for transport and dispersion coefficients are imported from another, conventional CFD simulation from the literature[4,8] based on calculations with the commercial CFD code FLUENT. The paper describes the numerical model, kept at the simplest form to be comparable to another model solution approach, which uses a new equivalent porous-media representation of the in-drift processes[9,15]. Numerical examples are included for the currently envisioned design and its variation of the proposed repository at YM.

A MULTI-SCALE, COUPLED NUMERICAL-COMPUTATIONAL MODEL

Model Concept

A specific aim of the model formulation is to describe the physical processes that contribute to the formation of a robust natural barrier to water reaching waste packages for

several thousands of years. The problem to be solved is the coupled, near-field and in-drift thermal, hydrologic, natural air movement, and condensation processes with mountain-scale effects at YM. The MF model is configured for a complete emplacement drift for the demonstration of the applicability and solvability the method for a complex and large example. The rockmass domain around an emplacement drift is selected to be large enough to include the connection between hot and cold drift sections. The in-drift moisture transport along the drift length as well as the condensate trapping process are modeled in three-dimensions (3-D) in order to describe the mechanism for moving water away from the waste packages towards the unheated drift-sections.

Thermal-hydrologic Model of the Rockmass

A multi-scale rockmass model is used to identify a representative NTCF model applying the TOUGH2 thermal-hydrologic porous-media code. A single drift is modeled in the example. Figure 1 shows the rockmass domain with an emplacement dr ift as a 3-D slice of the mountain in the middle of an emplacement panel. As depicted, the mountain slice that encaptures the drift stretches from the surface to the water table in the vertical z direction; from mid-point to mid-point between neighbor drifts in the horizontal x direction; and from unheated edge to unheated edge in the y direction. Sufficiently large unheated areas at both ends of the emplacement drift are included in the model domain. Rock properties and boundary conditions on the surface and at the water table are essentially identical to those of previous studies.[9,12]

The two undisturbed edge sections are passive heat and moisture sinks, facilitating edge cooling and condensate drainage via mountain-scale heat and moisture transport in the rock-mass. The emplacement drift is an open-volume, leaky air space around the waste packages, nearly infinite in permeability relative to that of the rock-mass. Inside the common air space,

two unheated drift sections are modeled, according to the baseline design for YM. These empty

drift sections have been found beneficial for condensing and draining vapor transported by

natural convection from the hotter, emplaced drift sections.[12]

A surrogate, NTCF rockmass model that describes the heat and moisture flow across the

rock-air interface is used in MF for coupling purposes. The NTCF model is determined using

nonlinear system identification.[3] The basic idea of the NTCF model-building is to fit a

mathematical model to the numerical TOUGH2 model. The fitting process uses numerical data,

which include inputs to, and outputs from the TOUGH2 model runs. The NTCF model

isrepresented by matrix equations with constant coefficient matrices, which may be considered

NTCF model constants. A pre-selected set of drift surface temperature, T, and partial vapor

pressure, P, variations are used as trial conditions in the TOUGH2 model to generate responses

for heat flux, qh, and moisture flux, qm, on the rock-air interface along the entire drift length and

over a post-closure time period of 5000 years. Along the length of the drift, 48 individual

mountain-scale divisions are applied of which only 24 are used in one TOUGH2 run, assuming

symmetry to mid-drift point. The relationship between the set of input T, P, and output qh, qm

temporal variations for each drift section i define the corresponding mountain-scale rockmass

NTCF model for heat and moisture. The following matrix equations are selected for the NTCF

model:

$$qh_i = qh_i^c + hh_i \cdot \left(T_i - T_i^c\right) + \langle T_i \rangle \cdot hm_i \cdot \left(P_i - P_i^c\right) \tag{1}$$

$$qm_i = qm_i^c + mh_i \cdot \left(T_i - T_i^c\right) + \langle T_i \rangle \cdot mm_i \cdot \left(P_i - P_i^c\right) \tag{2}$$

The hh_i, hm_i, mh_i, and mm_i dynamic admittance matrices are identified based on Eqs (1)

and (2) by fitting qh_i and qm_i to TOUGH2 data. The model for each drift-section perfectly

reproduces qh_i^c and qm_i^c, the central output fluxes from TOUGH2, for $T_i=T_i^c$ and $P_i=P_i^c$, the central input boundary conditions, that are included in the pre-selected set of boundary conditions.

Other T_i and P_i input variations can produce outputs from the NTCF model for qh_i and qm_i without actually re-running TOUGH2. Figure 2 shows comparison between the TOUGH2 and NTCF heat and moisture flux results for 24 models (i.e., for each of the 24 divisions along a half drift length) over a 5000 year time period. In Fig 2, the input T_i and P_i variations are +5% deviated from the T_i^c and P_i^c central values for which qh_i and qm_i vectors are calculated from Eqs. (1) and (2).

Within each 3-D mountain-scale rock cell ($i=1...24$), further divisions are made to capture the drift-scale temperature and humidity variations along the drift length and its circumference. For the coupled in-rock and in-drift model, the numerical discretization points on the drift wall are bundled into 3x454 averaged, independent surface nodes, 454 along the drift length and 3 in each section along the perimeter with respect to temperature and partial vapor pressure variations in the refined NTCF model. From the 24 mountain scale "parent" NTCF models, 3x454 drift scale "daughter" models are generated, following the technique used in other, previous studies[12-14]. Each mountain-scale rock cell for $i=1...24$ is re-scaled into j sub-divisions according to Table 1. The re-scaling of the hh_i, hm_i, mh_i, and mm_i mountain-scale 3-D cell matrices into drift-scale hh_{ij}, hm_{ij}, mh_{ij}, and mm_{ij} matrices are accomplished by proportioning them by the ratio between the ith cell and the ij^{th} drift segment surfaces, A_i and A_{ij}:

$$hh_{ij} = hh_i \cdot \frac{A_{ij}}{A_i} \tag{3}$$

$$hm_{ij} = hm_i \cdot \frac{A_{ij}}{A_i} \tag{4}$$

$$mh_{ij} = mh_i \cdot \frac{A_{ij}}{A_i} \tag{5}$$

$$mm_{ij} = mm_i \cdot \frac{A_{ij}}{A_i} \qquad (6)$$

The re-scaling procedure generates 3x454 individual drift-scale hh_{ij}, hm_{ij}, mh_{ij}, and mm_{ij} "daughter" matrices without any additional TOUGH2 runs, all inheriting the mountain-scale heat and moisture transport connections from the original, mountain-scale, "parent" matrices hh_i, hm_i, mh_i, and mm_i. The average size of the spatial rock domain in the axial drift direction is 1.7 m that is sufficient to generate temperature variations even along individual waste packages. The multi-scale NTCF rock model defines heat and moisture flux vectors as a function of the 3x454 time-dependent input vectors of surface temperature and partial vapor pressure boundary conditions, all considered unknown and subject to coupling calculations with the in-drift CFD model. The 3x454 nodes represent the interface boundary at the representative points between a rock cell and the airway that include the waste packages. The NTCF rock model includes both drift-scale and mountain-scale heat and moisture flow components without using any sub-models and subsequent superposition.

CFD Models for Heat and Moisture Transport in the Emplacement Drift

The lumped-parameter, in-drift CFD model configuration includes 80 m long, unheated sections, shown in Fig. 2, with heat and mass transport connections to the hot drift sections along them. A uniform heat load is assumed for each waste package in the drift, although this stipulation is not a necessity for the solvability of the model. The model is identical to those of a previous study[1012], applying two 80m unheated drift sections with no waste packages emplaced.

The energy balance equation in the CFD model of MF is used in a simplified form, as follows:

$$\rho c \frac{\partial T}{\partial t} + \rho c v_i \frac{\partial T}{\partial x} = \rho c a \frac{\partial^2 T}{\partial x^2} + \rho c a \frac{\partial^2 T}{\partial y^2} + \rho c a \frac{\partial^2 T}{\partial z^2} + q_h \qquad (7)$$

Equation (7) is written in the natural, streamline coordinate system of the flow field in which the velocity is x-directional, where x is tangent to the stream line. The average velocity is v_i in a flow channel of cross section dy by dz in the normal y and z directions to x.

In Eq. (7), ρ and c are density and specific heat of moist air, respectively, a is the molecular or eddy thermal diffusivity for laminar or turbulent flow, and q_h is the latent heat source or sink for condensation or evaporation. In turbulent shear and boundary layer flows, a is different in x, y, and z directions and may be substituted with direction-specific values for the effective dispersion coefficients together with its variation with temperature and location. The second and the third terms on the right-hand-side of Eq. (7) represent heat conduction (or effective heat conduction) in the normal, x and y directions to the x axis of the flow channel; these terms are substituted with expressions for transport connections using heat transport coefficients for flow channels bounded by solid walls. Eq. (7) is discretized and solved numerically and simultaneously along all flow channels for the temperature field T in MF. The flow channels represent the natural coordinate system of the flow field that must be known for the calculations.

The simplified moisture transport convection-diffusion equation in the CFD model of MF is similar to Eq. (7) as follows:

$$\frac{\partial \rho_v}{\partial t} + v_i \frac{\partial \rho_v}{\partial x} = D \frac{\partial^2 \rho_v}{\partial x^2} + D \frac{\partial^2 \rho_v}{\partial y^2} + D \frac{\partial^2 \rho_v}{\partial z^2} + q_{cm} + q_{sm} \qquad (8)$$

In Eq. (8), ρ_v is the partial density of water vapor, D is the molecular or eddy diffusivity for vapor (equated with the effective moisture dispersion coefficient in turbulent flow), q_{cm} is the moisture source or sink due to condensation or evaporation, and q_{sm} is the vapor flux in superheated steam form.

It is possible to reduce the number of discretization elements in the computational domain by lumping nodes. MF allows for defining connections between lumped volumes, applying direct heat and moisture transport relations between them. The current lumped-parameter CFD model in the drift applies 15x454 nodes for the heat, and the same number of nodes for the moisture transport. Each waste package is represented by two nodes, with one additional node for the gap between neighboring containers. CFD nodes are in the airway along three longitudinal lines: close to the drip shields, close to the drift wall above the drip shields, and close to the side wall, with 454 nodes on each line. The drift inside wall is assumed to be separated from the rock wall with a 10^{-5} m-thick still air layer, and are both represented by 454 nodes each along three lines: at the invert, sidewall, and roof. The sidewall and the crown of the drip shields are represented by two lines with 454 nodes on each. The airspace under the drip shields are modeled also by three lines each having 454 nodes. In addition, 3x454 nodes represent the rock-air interface, making the total number of nodes in the CFD model for heat 8172. The same number of nodes is used in the CFD model for moisture transport.

Figure 3 is a simplified illustration of both heat and moisture transport connections. Heat and moisture transport are modeled using heat and moisture transport coefficients at the waste package, drift wall, and at both sides of the drip shields. 3-D thermal radiation between solid surfaces is also included in the CFD models.

Natural, secondary air flow is considered due to the local temperature differences in the drift.   The mean axial airflow is assumed to be zero in the present case, unlike in a previous

study[13] in which a slow, axial in-drift airflow was assumed. Transport of heat and moisture in axial direction are modeled using constant dispersion coefficients adopted from the literature[4,5], published for a similar emplacement drift with axial thermal gradient ("with temperature tilt"), giving an axial dispersion coefficient of 0.1 m^2/s, and without axial thermal gradient ("without temperature tilt"), giving an axial dispersion coefficient of 0.004 m^2/s. In each drift segment of a half-waste package length, the re-circulating mass flow rate in the vertical direction is taken as 0.04 kg/s, a constant value for the study time period between 60 and 5,000 years, based on the FLUENT simulation results of natural convection studied by Webb and Itamura.[4,5] The mass flow rate in the vertical direction is used to calculate velocities along the air recalculation transport loops during the lumped-parameter CFD solution. The dominantly natural heat transport coefficient on the drift, waste package, and drip shield walls during post-closure are all set to a constant value of 1.85 W/(m^2K), a value consistent with the results of more detailed numerical modeling.[5]

Coupled In-rock NTCF and In-drift CFD Models

By iteration in an Inside Balance Iteration (IBI) cycle, the NTCF and CFD models are coupled on the rock-air interface. The IBI core process equates the heat and moisture flows at the common surface temperature and partial vapor pressure at each surface node and time instant. In the IBI core process, the fixed NTCF model provides temperature- and vapor concentration-dependent heat and mass fluxes on the rock-air interface. The NTCF model constants, i.e, the dynamic admittance matrices are kept unchanged, but the model results are variables.

The NTCF model, although nonlinear and best fit, cannot be considered perfect even in a small temperature and vapor concentration regime. Two main reasons necessitate NTCF model

update with re-functionalization: nonlinearities, different in characteristics from the nonlinear form used in Eqs. (1) and (2); and the effects of input components that are not explicitly modeled and functionalized for. Such implicit factors are the overall temperature and vapor concentration distributions on the drift surface along the drift length. The mountain-scale, axial heat and moisture flows affect the radial flows to some extent, which is only repeating the IBI process with a renewed NTCF model implicitly included in the NTCF model. A manual Outside Balance Iteration (OBI) may be performed in the current MF version. Figure 4 shows both the IBI and OBI processes. One IBI process provides a complete solution for the task, starting from an assumed solution, called the central values, T_c and P_c . Although they can be hypothetically arbitrary, a close-to-real selection for T_c and P_c obviously accelerates the convergence of the OBI process. The current example started from the balanced T_c and P_c results from an alternative solution using an integral TOUGH2 model with a porous-media in-drift model-element with effective, equivalent properties.[9,15]

The IBI core process is executed automatically in MF, providing coupled solution to the conjugate, multiphysics problem with two model-elements: the NTCF and the lumped-parameter CFD. The OBI, a manual process, is intended to update the NTCF surrogate model with new TOUGH2 results. The simulation results obtained from the CFD model elements are temperature, relative humidity, and water condensate variations within the emplacement drift, including distributions on the drift wall boundary. Temperature, humidity, and moisture flow distributions in the rockmass, already coupled to the in-drift processes, are given by the TOUGH2 porous-media model.

NUMERICAL RESULTS

Balanced results for the baseline case

Four OBI iterations have been completed, starting with initial conditions approximated from an alternative model that uses an equivalent porous-medium representation of the in-drift flow processes[9,15]. The final temperature and relative humidity results are shown in Fig 5, in 3-D plots in which the thick lines mark the position of the first and the last waste package in the drift. As shown, the relative humidity along the active emplacement area between the two thick lines is well below 100% saturation over the entire 5000 years.

Convergence of the OBI iterations

Starting from the results of the alternative model[9,15], as T_c^0 and P_c^0, four IBI processes were executed manually by repeating the cycles with updated T_c^{i+1} and P_c^{i+1} values according to the new balanced T^i and P^i results:

$$T_c^{i+1} = T^i \qquad (9)$$

$$P_c^{i+1} = P^i \qquad (10)$$

Note that each IBI iteration involved the entire 5000 years study period. It will be more economical to use OBI iterations time-step by time-step in future applications. However, the OBI still involves a manual process of running TOUGH2 in the current MF version, and reducing the manual interactions to only four made it desirable for packaging the task for the long time period. The convergence of the IBI iteration results is depicted in Figure 6 a through c for temperature and heat wall flux for the hottest and coldest drift sections. The dashed lines are the starting T_c distributions in Figures 6a and b, while the thick lines are the final, balanced results. As shown, the iterations converge fast and little change is made after the first step. The same tendency is shown for heat flux, qh_c, for both hot and cold drift sections: the first iteration result hardly changes ever after, indicating that the NTCF model captures the in-rock processes

excellently. There are residual differences between the MF-based results and those from an alternative model[9, 15], to be discussed later in the paper.

The convergence of the IBI iteration results is shown in Figure 7 a through f for partial vapor pressure, moisture flux, and condensation rates for the hottest and coldest drift sections. The variations between iteration steps are larger than for heat, an indication of stronger non-linearities. The convergence is still fast for both partial vapor pressure and moisture flux for the hot sections. The cold section results for moisture flux show the strongest variations during consecutive OBI iterations. The magnitude of the wall moisture flux is, however, small relative to the total moisture transport on the same drift wall due to condensation, as seen by comparing the scales of sub-figures 7 d and f. The insignificance of the small amount of moisture flux on the cold drift sections explain the fact that the partial vapor pressure variations are much less variable and show a converging settlement in spite of the widely alternating moisture flux results between iterations. The residual deviations between the MF (solid lines) and the approximate representation of the alternative model that was used as the starting point for the iterations (dashed lines) are also larger for moisture flux and vapor pressure than for the heat flux and temperature.

Fast convergence provides confirmation of the NTCF modeling approach. With no mountain-scale effects and only linear processes, theoretically, only one IBI process (and no OBI iteration) would be needed[3]. The transport processes at YM with the high-temperature operating mode (HTOM) can still be reasonably captured with the NTCF model for sensitivity and other scoping calculations without applying OBI iterations.

Following this conclusion, the study was repeated without changing the NTCF model for a modified drift arrangement in which the moisture transport was blocked by impermeable seals at the first and last waste packages, shown in Fig 8. The effect of the blockages is simulated in

the CFD model by eliminating the axial moisture transport connections between the heated and unheated drift sections at two given locations. These blockages are assumed to cut moisture transport from the hot, emplaced drift section to the cold, empty drift sections. The thermal connections were not changed in the model. Figure 9 a and b are temperature and relative humidity distributions in 3-D format for the drift arrangement with sealed-off unheated sections. As shown, the relative humidity along the drift length is not monotonous: saturation peaks to 100% first within the active emplacement section, and peaks again in the unheated section.

Temperature, relative humidity, and condensate distributions along the drift length at six time instants are shown in Figure 10 a, b and c for both un-sealed (solid lines) and sealed-off unheated drift sections (dashed lines). As shown, the long, unheated drift sections significantly reduce the relative humidity in the emplacement drift along the waste packages. No condensation is found on the wall, drip shield, or waste packages within the study time period in the active emplacement drift section. In comparison, the arrangement with no unheated drift sections shows significantly higher relative humidity distribution along the active drift section. However, only the locations of the two coldest waste packages develop condensation, acting as drainage sinks in the emplacement drift.

Comparison with alternative model results

Comparison of the thick solid and the thick dashed lines in Figs. 6 and 7 demonstrates that there are residual differences between MF and the alternative equivalent porous-medium model that was used as a starting point for the iterations[9,15]. These differences are not unrealistically high when considering (1) that the MF model results are preliminary in nature as the iterations are still ongoing and (2) that the alternative model results were deliberately perturbed by averaging over the drift perimeter and coarsening the time step subdivision, in order to provide a more challenging iteration task for MF. In addition, there are differences in

discretization (with much finer in-drift gridding in the MF model) as well as differences in the representation of in-drift design features, with the drip shield included in the MF model, but omitted in the alternative model. However, even without the above factors, there would never be a perfect match between the two modeling approaches because of the fundamental differences in the treatment of the in-drift flow processes.

Let us briefly discuss some of the approximations necessary in the equivalent porous-medium representation of the in-drift flow processes, as implemented in the alternative model[9,15]. The equivalent porous-medium representation assumes dominantly diffusive-dispersive and conductive transport mechanisms in the drift; laminar fluid flow, as part of the TOUGH2 solution, is incorporated in the airspace. For computational reasons, the permeability of the airway, which may be on the order of 0.2 m^2 in laminar flow, needs to be approximated with a much smaller value of about 10^{-8} m^2. Note that the average permeabilities of the surrounding rockmass are typically 10^{-13} m^2 for fractures and 10^{-17} m^2 for the pore matrix at YM. Thus using a value of 0.2 m^2 would represent a very large contrast within one model, leading to extreme computational difficulty in a porous-medium representation. The MF model, on the other hand, allows for a realistic representation of such large air-space permeability values, because the in-drift and the rock mass are treated as separate model elements. Note also that the MF model represents the strong axial mixing process using an explicit velocity field in the vertical cross sections. In the equivalent porous-medium representation, in contrast, the transport of heat and moisture by concentration and temperature gradients is approximated with bi-directional diffusion-dispersion terms, assumed identical in axial and radial direction. Convective transport in the air space is not modeled, missing the directional effects caused by transport velocities. A previous study compared and found significant differences in the condensation patterns between

models using an equivalent dispersive transport model and the other using convection model elements with transport velocities.[13]

In conclusion, different results should be expected from the equivalent porous-medium models[9,15] when compared to the MF model, even if the same model setup with the same discretization, the same rockmass properties, and the same in-drift transport coefficients were used. An equivalent porous-medium model, such as described in Birkholzer et al.[9,15], should be viewed as a robust direct method for arriving at approximate solutions for the coupled in-drift rock mass system. The new MF model developed in this paper, on the other hand, is a more complex model that allows for significantly more detail and realism in representing the in-drift flow and transport patterns.

Low Axial Dispersion Case, Sealed and Un-sealed Unheated Drift Sections

As another solution example, a low axial dispersion coefficient of 0.004 m^2/s was also selected[4,5] for a comparative study. The study with the low dispersion coefficient included again two model runs, one with the unsealed, unheated end sections to establish baseline results, and one with the seals in the moisture transport model. The results of the low axial dispersion coefficient study are shown in Figure 11a, b and c for temperature, relative humidity, and condensate at six selected time instants. Results for the baseline and the sealed-off arrangements are shown respectively, in solid and in dashed lines in Figures 11 a, b and c. As depicted, the benefit of long, unsealed, unheated drift section in the emplacement drift is not as strong in the low axial dispersion case as in the one with high axial dispersion coefficient. If the axial transport is not strong enough for carrying away the vapor and superheated steam from the hot drift section to the cold ends, the relative humidity is not reduced considerably in the middle drift section by the axial moisture transport. Condensation is predicted at some cold spots such as at

the gaps between waste packages. However, some benefits are still seen in humidity and seepage/condensate reduction.

Discussion of the Dispersion Coefficient Model

The high sensitivity of vapor transport results to the value of the axial dispersion coefficient warrants close attention. Within the drift airspace, stagnant, as well as highly turbulent airflow domains are present, depending on the natural buoyancy driving forces caused by temperature differences in a particular location. The molecular diffusion coefficient for air in an air-vapor mixture is D_0 = 2.13 x 10^{-5} m^2/s [2], while the overall, average, axial dispersion coefficient in a turbulent, mixing flow may be as high as 0.1 m^2/s. [5,4] These values, over-arching three orders of magnitude, co-exist in an emplacement drift. It will be highly desirable to apply location- and temperature-specific dispersion coefficient values in the lumped-parameter CFD model in the future.

A possible solution is to determine a numerical-empirical relationship between the axial dispersion coefficient and the axial temperature difference for the axial convection cells, in non-dimensional form based on existing data[5,4] and/or new FLUENT simulations. The lumped-parameter CFD model in MF then can be used to incorporate location- and temperature-dependent values in the coupled model solution. An example of such a non-dimensional expression for the dispersion coefficient may be obtained by fitting the following model to published data[5,4]:

$$D = D_0 \left\{ 1 + 76 Ra_{L_C, \Delta T_r}^{0.05} \left[1 + 0.05 \left(\frac{L_C}{L} \right) Ra_{L_C, \Delta T_L}^{0.5} \right] \right\} \tag{11}$$

In Eq. (11), the following relationships are used:

$$D_0 = 2.158/P_b \tag{12}$$

$$Ra_{L_C, \Delta T_r} = \frac{g\beta \cdot \Delta T_r \cdot L_c^{\ 3}}{v \cdot a} \tag{13}$$

$$Ra_{L_C, \Delta T_L} = \frac{g\beta \cdot \Delta T_L \cdot L_c^{\ 3}}{v \cdot a} \tag{14}$$

In Eq (11), $Ra_{Lc,\Delta Tr}$, is the Rayleigh number calculated with the gap-width characteristic length[5,4], L_C, and temperature difference in radial direction; and $Ra_{Lc,\Delta TL}$, is the Rayleigh number calculated with the same characteristic length but with a temperature difference over the axially connected distance, L, along the drift length. Equation (11) fits quite well to existing data[5,4] shown in Table 2. The model may reduce CFD input uncertainty from three orders of magnitude to a few tens of percent.

CONCLUDING REMARKS

Numerical examples are presented with a refined iterative model using MF with a TOUGH2 model for the rock-mass, and a lumped-parameter CFD in-drift model for the air space are used. Air and vapor flows are allowed in the drift space in which the barometric pressure is kept at an approximately constant value within 10 Pa variation. The model captures the processes driven by temperature, total pressure, and humidity concentration differences. The results represent the first of this kind of solution for the baseline design case for YM. The model still has room for improvements and refinements. The constant axial dispersion coefficient D is one of the uncertain elements in the model. Neither a low nor a high constant value for D is realistic for the entire drift length. It will be necessary to keep D as a variable coefficient, e.g., after verification, using Eq.11. Other refinements are planned with the use of a variable, updated air velocity and surface transport coefficients distributions. These modifications in the model

configuration will affect the numerical results, and may require a larger number of OBI iterations.

The MF model converged robustly during IBI iterations in a large and complex task that involved a full, 3-D emplacement drift and a large, enclosing rock mass with added, unheated edge areas. A few OBI iterations seem to be sufficient for correcting the solution due to strong nonlinearities in moisture transport and changing mountain-scale effects in a high-temperature test example.

As a coupled thermal-hydrologic model exercise, the beneficial effect of elongated, unheated emplacement drift sections at both ends was studied and comparatively evaluated without OBI model repetitions. No condensation was found around the waste packages, and an improvement to the results for a drift arrangement without the long unheated sections was achieved in the high axial dispersion coefficient case.

Lower condensation rates and fewer condensation locations in the emplacement drift are predicted with the present model than those obtained using an approximate, and basically un-coupled condensation model[5].

The application of an unheated drift section for decreasing humidity in the emplacement drift has been studied before[17], although in a different arrangement in which a slow air re-circulation along the drift was engineered. The current result once again illustrates the benefit of maintaining unheated, low-temperature sections in the drift airspace in order to lower the relative humidity in the active emplacement drift section. Significant sensitivity to the axial dispersion coefficient in the emplacement drift is found. This result underlines the importance of a fast-running, efficient modeling method, since input data variations will likely be needed in future studies and design exercises.

The range of the values for axial dispersion coefficient arches over three orders of magnitude from molecular diffusion to turbulent dispersion in an emplacement drift. In order to reduce uncertainties, it will be important to use location-specific, temperature field dependent coefficients in the lumped-parameter CFD model instead of overall constants for the entire drift in future studies. Such a dispersion coefficient model example is given in Eq (11), derived as a fitting exercise.

ACKNOWLEDGMENTS

NOMENCLATURE

A cross section

A_{ij} ij^{th} cell drift segment surface

A_i i^{th} cell drift segment surface

a molecular or eddy thermal diffusivity for laminar or turbulent flow

c specific heat of moist air

D_0 molecular diffusion coefficient for air in an air-vapor mixture

D molecular or eddy diffusivity or dispersion coefficient

g gravitational constant

hh_i i^{th} rock cell temperature-driven admittance matrix of heat flux

hh_{ij} ij^{th} drift segment temperature-driven admittance matrix of heat flux

hm_i i^{th} rock cell vapor pressure-driven admittance matrix of heat flux

hm_{ij} ij^{th} drift segment pressure-driven admittance matrix of heat flux

L characteristic length along the drift

L_C half gap-width characteristic length in drift cross section $= 2A/P$,

mh_i i^{th} rock cell temperature-driven admittance matrices for the moisture flux

mm_i i^{th} rock cell vapor pressure-driven admittance matrices for the moisture flux

mh_{ij} ij^{th} drift segment temperature-driven admittance matrices for the moisture flux

mm_{ij} ij^{th} drift segment vapor pressure-driven admittance matrices for the moisture flux

P_b barometric pressure

P partial vapor pressure vector

P_i i^{th} rock cell partial vapor pressure vector

P^c_i i^{th} rock cell partial vapor pressure variation vector (central condition around which the

NTCF model is determined).

P_s saturated vapor pressure

q_{cm} moisture source or sink due to condensation or evaporation

qh_i i^{th} rock cell heat flux vector

qh^c_i i^{th} rock cell heat flux variation vector (central condition around which the NTCF model

is determined).

q_h latent heat source or sink for condensation or evaporation

qm_i i^{th} rock cell moisture flux vector

qm^c_i i^{th} rock cell moisture flux variation vector (central condition around which the NTCF

model is determined).

q_{sm} vapor flux in superheated steam form

$Ra_{L_C, \Delta T_r}$ Rayleigh number at L_C and ΔT_r

$Ra_{L_C, \Delta T_L}$ Rayleigh number at L_C and ΔT_L

T temperature field

T_i i^{th} rock cell temperature vector

T^c_i i^{th} rock cell temperature variation vector (central condition around which the NTCF

            model is determined).

ΔT_r temperature difference in radial direction in a drift cross section

ΔT_L temperature difference over longitudinal distance L,

t time vector

x, y, z Cartesian coordinate system

Greek

ρ density of moist air

ρ_v partial density of water vapor

β coefficient of thermal expansion of moist air

ν kinematic viscosity of moist air

REFERENCES

[1] DOE, 1996. "Thermal Loading Study for FY 1996." B00000000-01717-5705-00044 REV 01. Las Vegas, Nevada: CRWMS M&O. ACC: MOL.19961217.0121.

[2] Pruess, K., C. Oldenburg, and G. Moridis, 1999. "TOUGH2 User's Guide, Version 2.0." Report LBNL-43134, Lawrence Berkeley National Laboratory, Earth Sciences Division, Berkeley, California.

[3] Danko, G., 2006. "Functional or Operator Representation of Numerical Heat and Mass Transport Models." Journal of Heat Transfer, February 2006, Vol. 128, 162-175.

[4] Bechtel SAIC Company, 2004. "In-drift natural convection and condensation." Yucca Mountain Project Report, MDL-EBS-MD-000001 REV 00, Bechtel SAIC Company, Las Vegas, NV.

[5] Webb, S. W. and Itamura M. T., 2004. "Calculation of Post-Closure Natural Convection Heat and Mass Transfer in Yucca Mountain Drifts." Proceedings of ASME, Heat Transfer/Fluid Engineering, July 11-15, Charlotte, NC.

[6] Hao, Y. Nitao, J.J., Buscheck, T.A. and Sun, Y., 2006. "Double Diffusive Natural Convection in a Nuclear Waste Repository." Proceedings, 11th International High-Level Radioactive Waste Management Conference, Las Vegas, NV, pp. 615-622.

[7] United States Department of Energy (DOE), 2004. "Multiscale Thermohydrologic Model, Report." Prepared by Bechtel SAIC Company, ANL-EBS-MD-000049 REV 01, LasVegas, NV.

[8] Francis, N.D., Jr.; Webb, S.W.; Itamura, M.T.; and James, D.L. 2003. "CFD Modeling of Natural Convection Heat Transfer and Fluid Flow in Yucca Mountain Project (YMP) Enclosures." SAND2002-4179. Albuquerque, New Mexico: Sandia National Laboratories.ACC: MOL.20030906.0165.

[9] Birkholzer, J., N. Halecky, S.W. Webb, P.F. Peterson, G.S. Bodvarsson, 2006. "The Impact of Natural Convection on Near-Field TH Processes at Yucca Mountain." Proceedings, 11th International High-Level Nuclear Waste Conference, April, Las Vegas, NV.

[10] Danko, G. and Bahrami, D. 2005. "Coupled Hydrothermal-Ventilation Studies for Yucca Mountain Annual Report For April 2004-March 2005." NWRPO-2005-02. Prepared for Nye County Department of Natural Resources and Federal Facilities. Pahrump, NV.

[11] Birkholzer, J., S. Mukhopadhyay, Y.W. Tsang, 2004. "Modeling Seepage into Heated Waste Emplacement Tunnels in Unsaturated Fractured Rock." Vadose Zone Journal, 3, 819-836.

[12] Danko, G., Birkholzer, Bahrami, D., 2006. "The Effect of Unheated Sections on Moisture Transport in the Emplacement Drift." Proceedings, 11th International High-Level Nuclear Waste Conference, April, Las Vegas, NV.

[13] Danko, G., Bahrami, D., 2004. "Coupled, Multi-Scale Thermohydrologic-Ventilation Modeling with MULTIFLUX ," 2004 SME Annual Meeting, February 23-25, Denver, CO.

[14] Bahrami, D. and Danko, G., 2006. "Thermal-Hydrologic Model of an Alternative Waste Package Design for Yucca Mountain Repository." Journal of Nuclear Technology, May, Vol. 154.

[15] Birkholzer, J.T., Webb, S.W., Halecky, N., Peterson, P.F. and Bodvarsson, G.S., 2005. "Evaluating the Moisture Conditions in the Fractured Rock at Yucca Mountain: The Impact of Natural Convection Processes in Heated Emplacement Drifts." LBNL-59334, Berkeley, CA, Lawrence Berkeley National Laboratory.

[16] Buscheck, T.A., Sun, Y. and Hao, Y., 2006. "Multiscale Thermohydrologic Model Supporting the License Application for the Yucca Mountain Repository." Proceedings, 11th International High-Level Radioactive Waste Management Conference, Las Vegas, NV, pp. 737-746.

[17] DOE, 1999. "Design Alternative Evaluation #3: Post-Closure Ventilation." Civilian Radioactive Waste Management System Management & Operating Contractor, BCA000000-01717-2200-00003 Rev 00.

TABLES

Table 1. Drift-scale NTCF subdivisions in each mountain-scale rock cell.

I	j	i	J	i	j	i	J
1	3x7	7	3x6	13	3x1	19	3x4
2	3x4	8	3x5	14	3x3	20	3x6
3	3x6	9	3x3	15	3x3	21	3x12
4	3x6	10	3x3	16	3x3	22	3x23
5	3x6	11	3x3	17	3x5	23	3x45
6	3x6	12	3x3	18	3x3	24	3x61

Table 2. Comparison of dispersion coefficient values (m^2/s) between Equation (11) and published results[4,5]

		Without Temperature Tilt		With Temperature Tilt	
		1000 Yrs	3000 Yrs	1000 Yrs	3000 Yrs
Under Drip Shield	From [4,5]	0.006	0.007	0.007	0.009
	From Eq(11)	0.004	0.004	0.009	0.008
Outside Drip Shield	From [4,5]	0.004	0.004	0.1	0.1
	From Eq(11)	0.004	0.004	0.1	0.081

Figure 1. Rockmass domain around an emplacement drift in an emplacement panel 2.
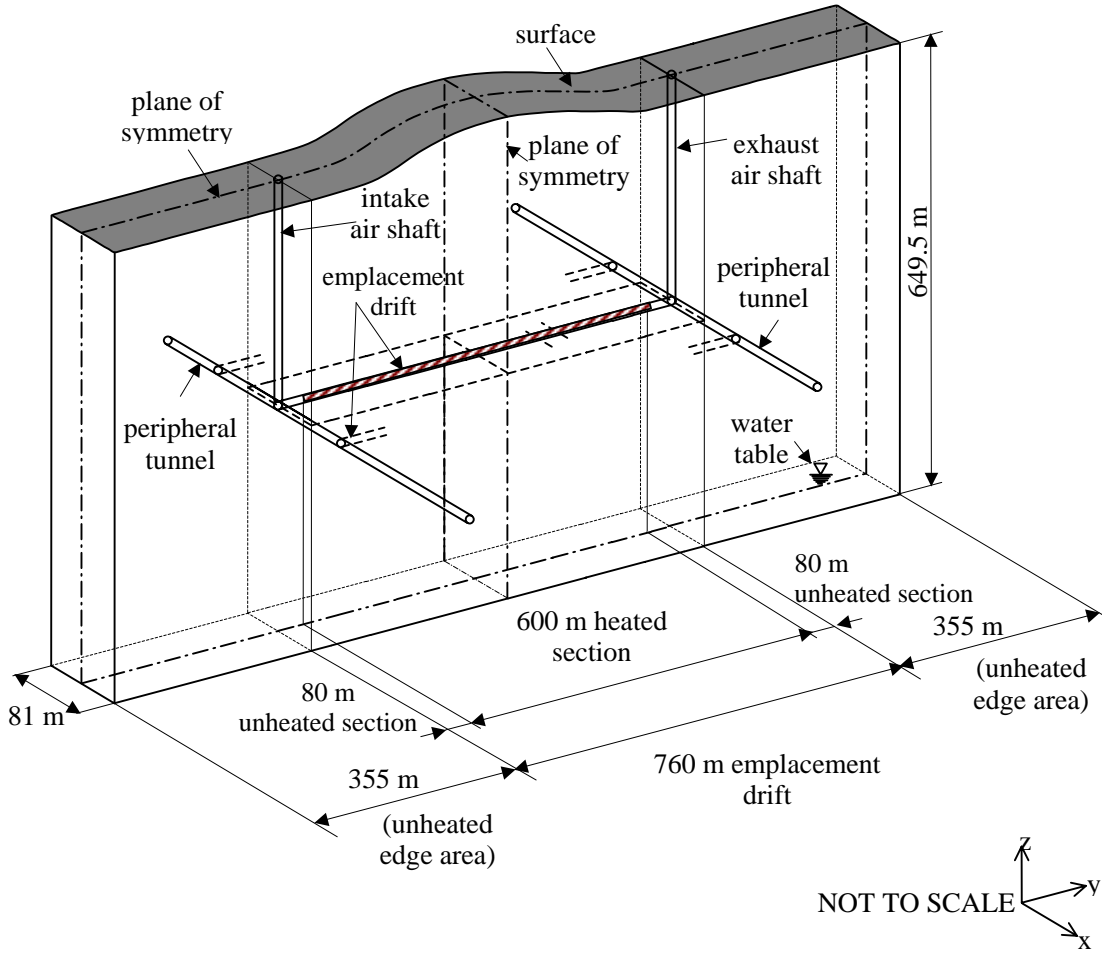
Heat Flux along the Drift (W/m)

Moisture Flux ₓ 10⁶ along the Drift (kg/s-m)
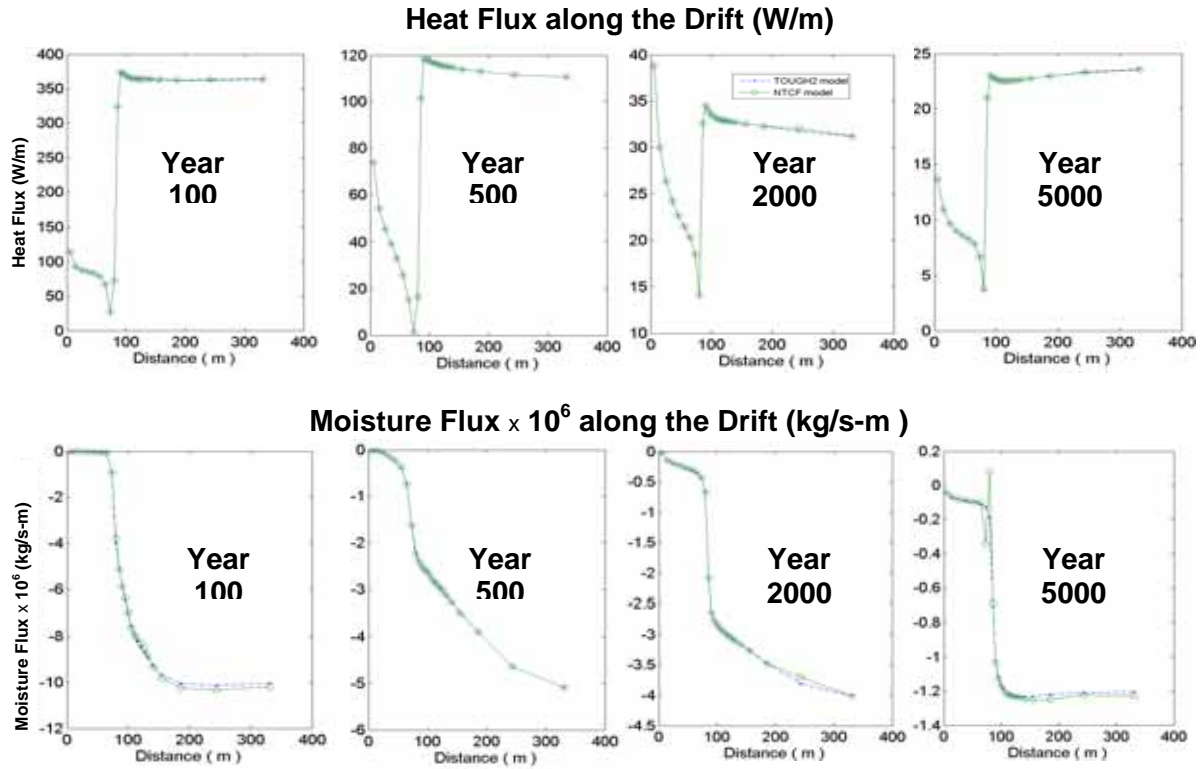
Figure 2. Comparison between the heat and moisture flux results from TOUGH2 and the NTCF model. The 24 points along a half-drift length in the heat and moisture flux curves are from 24 individual NTCF models. Note that the first 80 m of drift section has no waste packages.

Figure 3. In-drift lumped parameter CFD; for heat in axial direction (a); for heat in A-A cross section (depicted only on the left-hand-side of the symmetrical figure) (b); for moisture in axial direction (c); and for moisture in A-A cross section (d) (depicted only on the left-hand-side of the symmetrical figure).

Figure 4. The inside and outside balance iteration processes in MULTIFLUX.

Figure 5. Drift wall temperature (a); and relative humidity distributions (b) for case of unheated sections not sealed. The a axial moisture dispersion coefficient is 0.1 m²/s.

Figure 6. Temperature and heat flux convergence during four outside balance iterations for the hottest and coldest drift sections.

Figure 7. Vapor pressure, moisture flux, and condensation rate convergence during four outside balance iterations for the hottest (a, c, d) and coldest (b, d, f) drift sections.

Figure 8. Sectional view of the emplacement drift for the case of unheated sections not sealed (a); and unheated section sealed off (b).
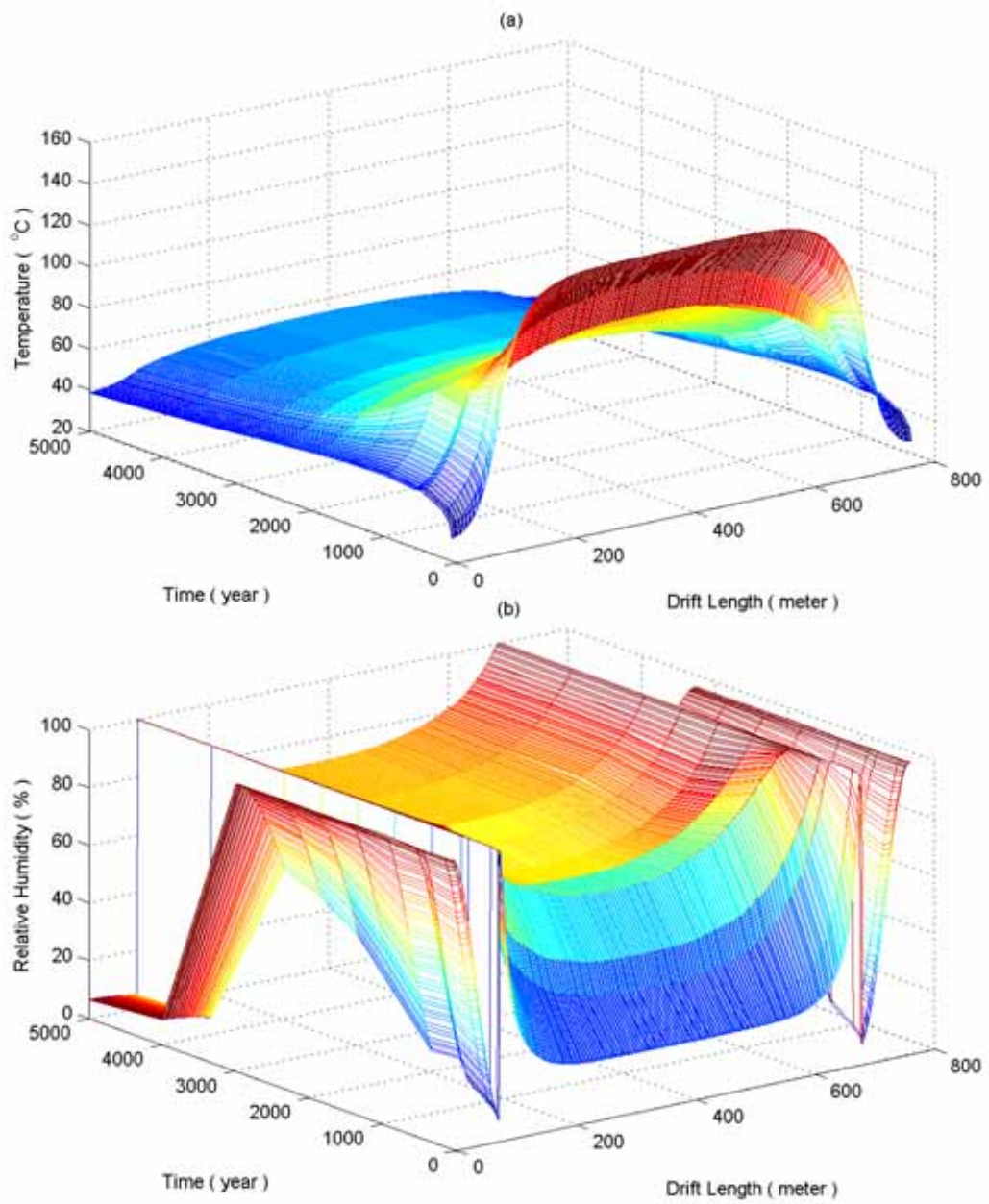
Figure 9. Drift wall temperature (a); and relative humidity distributions (b) for case of unheated sections sealed off. The axial moisture dispersion coefficient is 0.1 m^2/s.
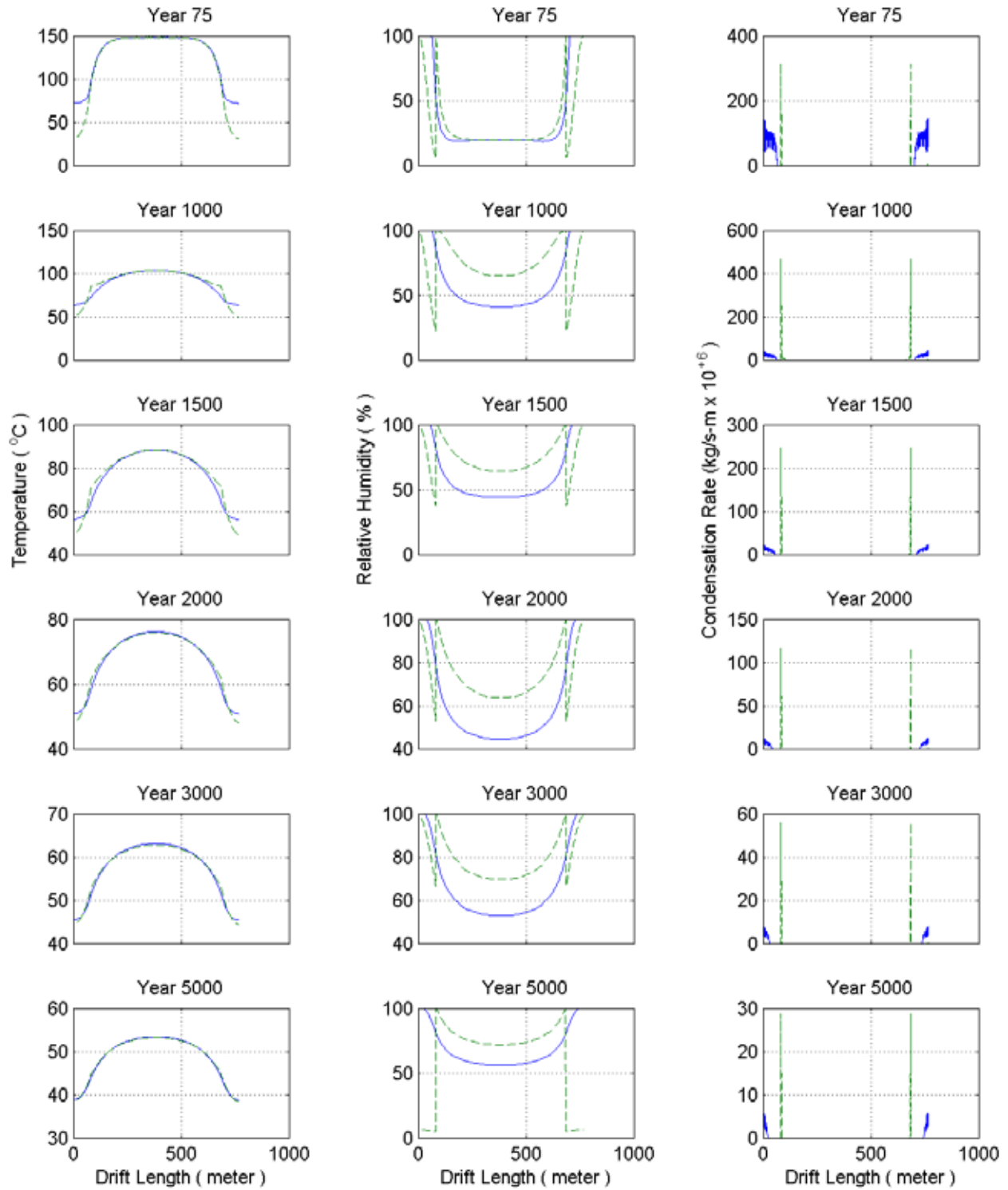
Figure 10. Axial distribution of (a) drift wall temperature, (b) relative humidity, and (c) condensation rate at selected post-closure time divisions using an axial moisture dispersion coefficient of 0.1 m²/s (solid line for the case of unheated sections not sealed and dashed line for the case of unheated sections sealed off).
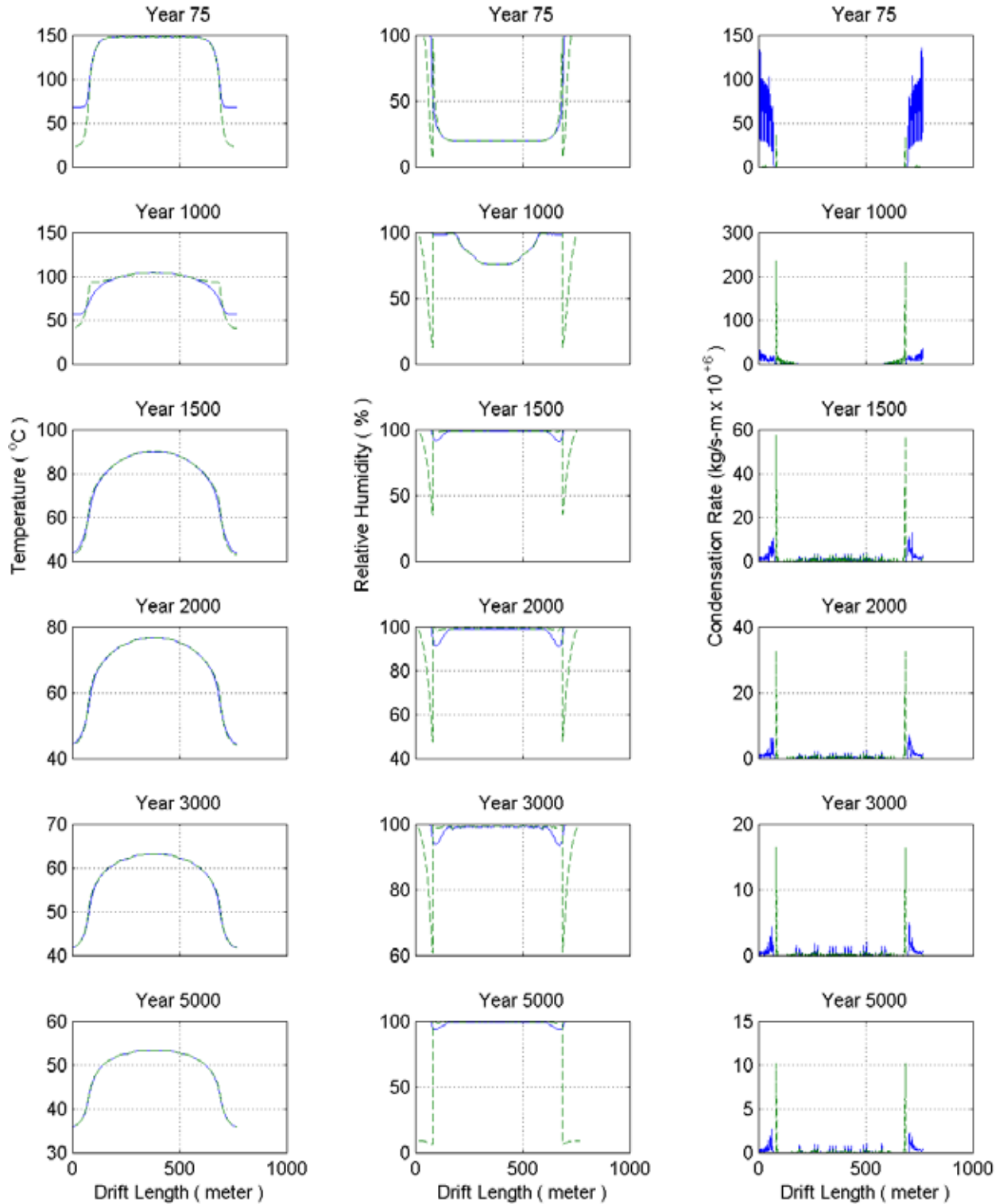
Figure 11. Axial distribution of (a) drift wall temperature, (b) relative humidity, and (c) condensation rate at selected post-closure time divisions using an axial moisture dispersion coefficient of 0.004 m²/s (solid line for case of unheated sections not sealed, and dashed line for case of unheated sections sealed off).

FIGURE CAPTIONS

Figure 1. Rockmass domain around an emplacement drift in an emplacement panel 2.

Figure 2. Comparison between the heat and moisture flux results from TOUGH2 and the NTCF model. The 22 points along a half-drift length in the heat and moisture flux curves are from 22 individual NTCF models. Note that the first 80 m of drift section has no waste packages.

Figure 3. In-drift lumped parameter CFD; for heat in axial direction (a); for heat in A-A cross section (depicted only on the left-hand-side of the symmetrical figure) (b); for moisture in axial direction (c); and for moisture in A-A cross section (d) (depicted only on the left-hand-side of the symmetrical figure).

Figure 4. The inside and outside balance iteration processes in MULTIFLUX.

Figure 5. Drift wall temperature (a); and relative humidity distributions (b) for case of unheated sections not sealed. The a axial moisture dispersion coefficient is 0.1 m^2/s.

Figure 6. Temperature and heat flux convergence during four outside balance iterations for the hottest and coldest drift sections.

Figure 7. Vapor pressure, moisture flux, and condensation rate convergence during four outside balance iterations for the hottest (a, c, d) and coldest (b, d, f) drift sections.

Figure 8. Sectional view of the emplacement drift for the case of unheated sections not sealed (a); and unheated section sealed off (b).

Figure 9. Drift wall temperature (a); and relative humidity distributions (b) for case of unheated sections sealed off. The axial moisture dispersion coefficient is 0.1 m^2/s.

Figure 10. Axial distribution of (a) drift wall temperature, (b) relative humidity, and (c) condensation rate at selected post-closure time divisions using an axial moisture dispersion coefficient of 0.1 m^2/s (solid line for the case of unheated sections not sealed and dashed line for the case of unheated sections sealed off).

Figure 11. Axial distribution of (a) drift wall temperature, (b) relative humidity, and (c) condensation rate at selected post-closure time divisions using an axial moisture dispersion coefficient of 0.004 m^2/s (solid line for case of unheated sections not sealed, and dashed line for case of unheated sections sealed off).

TABLE TITLES

Table 1. Drift-scale NTCF subdivisions in each mountain-scale rock cell.

Table 2. Comparison of dispersion coefficient values (m^2/s) between Equation (11) and published results[4,5]